Effect of Chain Architecture on Surface Segregation in Functional Polymers: Synthesis and Surface Properties of End- and Center-Functional Poly(D,L-lactide)

Derek A. Wong,[†] Patricia A. V. O'Rourke-Muisener,[‡] and Jeffrey T. Koberstein*[,§]

The Polymer Program, Institute of Materials Science, University of Connecticut, Storrs, Connecticut 06269-3136, Chemistry Department, University of South Florida, 4202 E. Fowler Avenue, SCA 400, Tampa, Florida 33620-5250, and the Department of Chemical Engineering, Columbia University, 500 West 120th Street, New York, New York 10027

Received March 27, 2006; Revised Manuscript Received October 5, 2006

ABSTRACT: Poly(D,L-lactide)s with fluorocarbon functional groups located at either the chain end or center are synthesized by the ring-opening solution polymerization of D,L-lactide using monohydroxy or dihydroxy terminated semifluorinated alcohols as co-initiators respectively. The surface composition−depth profiles of the fluorocarbon functional groups are determined by angle dependent X-ray photoelectron spectroscopy (ADXPS) measurements. All polymers exhibit surface segregation of the lower surface tension fluorocarbon functional groups. The extent of surface segregation decreases with molecular weight and, for polymers of equivalent molecular weight, is higher for the end-functional polymers than for center-functional polymers, consistent with the mean field lattice model (MFLM) predictions of O'Rourke-Muisener et al. We find that the MFLM with a single set of bulk and surface interaction parameters provides reasonable predictions of experimental ADXPS concentration depth profiles for all molecular weights and polymer architectures studied. Moreover, these interaction parameter values are in good agreement with those calculated by group contribution methods based upon the chemical structure of the functional groups.

Introduction

Surface properties are generally critical to the end-use and final performance of materials and engineered devices employed in many technological applications. These include properties related to adhesion (e.g., wettability, adhesive bonding, and releasability), wear (e.g., friction, and lubricity), optical applications (e.g., opacity), and biocompatibilty (e.g., cell adhesion). In multicomponent polymers, the composition and properties at the surface generally differ from those in the bulk material as a result of a phenomenon referred to as surface segregation. Components of lowest surface tension segregate preferentially to the surface in order to lower the surface energy of the material. Because the surface properties of a polymer are directly related to the surface composition, it is therefore of broad interest to develop a quantitative understanding of the surface segregation phenomenon and how it depends upon the thermodynamic properties of the constituents and the architecture of multicomponent polymers. The general phenomenon of surface segregation has been well documented in a wide variety of chemically heterogeneous polymer systems.[1−15]

Polymers of controlled architecture, such as end-functional polymers, are a particularly interesting class of materials that are known to exhibit surface segregation. They not only serve as convenient model systems that reflect the general behavior of all functional polymers, but also constitute a practical means for modifying surface properties without affecting substantial changes in the bulk properties. Surface segregation has been studied with an assortment of experimental techniques for a number of end-functional polymer systems in both neat form and their blends with a nonfunctional homopolymer.[8,9,11−13,16−19] These works demonstrate surface enrichment for end groups of lower surface tension than the chain backbone and surface depletion for end groups of higher surface tension.

Lattice models have been shown to provide excellent representation of the surface properties of end-functional poly(dimethylsiloxane)[7] and polystyrene[18] (PS), as well as block and random copolymers.[20] The lattice model has also proven successful in reproducing experimental functional group concentration depth profiles for ω-fluorosilane functional PS and its blends with nonfunctional PS determined by angle-dependent X-ray photoelectron spectroscopy (ADXPS) measurements.[17]

In recent work, we have used the lattice model to investigate the effects of chain architecture on the properties of functional polymer surfaces[16] and have shown how this information leads to several fundamental principles for their molecular design.[21] One of the many important predictions of the lattice model is that low-energy functional groups located at the chain ends segregate more efficiently to the surface than do functional groups located at the center of the chain. These calculations suggest that an end-functional architecture should therefore be most efficient for creating a macromolecular surfactant because it provides for optimal reduction in surface tension. If the predictions of the lattice model can be verified, it becomes an important tool that can be used to design optimal polymer architectures for specific surface applications. The influence of chain architecture on the surface properties of functional polymers has yet to be studied experimentally in any detail, however, in part due to the difficulty in synthesizing well-characterized functional polymers of varying architectures.

* Corresponding author: E-mail: jk1191@columbia.edu. Telephone: 212-854-3120. Fax: 212-854-3054.

[†] Current address: Ciba Specialty Chemicals, 540 White Plains Rd., Tarrytown, NY 10591.

[‡] Current address: Chemistry Department, University of South Florida, 4202 E. Fowler Avenue, SCA 400 Tampa, FL 33620-5250.

[§] Current address: Department of Chemical Engineering, Columbia University, 500 West 120th Street, New York, NY 10027.

10.1021/ma0606915 CCC: $37.00
Published on Web 02/02/2007

In this paper, we report the synthesis and characterization of a series of model end-functional and center-functional poly(D,L-lactide)s incorporating fluorocarbon functional groups. Experimental functional group concentration depth profiles are determined by ADXPS and are used to test the ability of mean-field lattice model (MFLM) calculations to predict the dependence of functional polymer surface properties on chain architecture.

Experimental Methods

Materials. 3,6-Dimethyl-1,4-dioxane-2,5-dione (D,L-lactide) and tin(II) 2-ethyl hexanoate ($Sn(Oct)_2$) were purchased from Aldrich. The D,L-lactide was recrystallized from ethyl acetate and vacuum-dried at 30 °C for at least 2 days prior to use. $Sn(Oct)_2$ was used as received. 1*H*,1*H*,2*H*,2*H*-perfluoro-1-decanol (98%), and 1*H*,1*H*,-10*H*,10*H*-perfluoro-1,10-diol (96%) were obtained from Lancaster Chemicals and used without further purification. Methanol (extra dry grade), toluene (extra dry grade), hexanes (HPLC grade), ethyl acetate, and tetrahydrofuran (uninhibited) (THF) were obtained from Acros Chemicals and used as received.

Synthesis Procedure. Poly(D,L-lactide)s with fluorocarbon functional groups located at either the chain end or center were synthesized by the ring-opening solution polymerization of D,L-lactide using monohydroxy or dihydroxy terminated semifluorinated alcohols as co-initiators respectively. Monomer, co-initiator and $Sn(Oct)_2$ catalyst were weighed into a previously flame-dried 50 mL two neck round-bottom flask containing a magnetic stir bar at room temperature. The flask was sealed using rubber septa and purged with dry nitrogen for 10 min. 30 mL of dry toluene was then charged into the flask via cannula and the flask immersed in an oil bath preheated to 100 °C. Temperature control was ±5 °C. The reaction was allowed to proceed for times ranging from 12 to 16 h, depending on the target molecular weight. The reaction solution was concentrated using a vacuum line and then precipitated into 500 mL of hexanes and allowed to stand overnight in a fridge maintained at 4 °C. After the overnight settling period, two more precipitations were performed into hexanes using THF as the solvent. The polymer product was subsequently dried in a vacuum oven at 35 °C for 3 days before use.

Nuclear Magnetic Resonance. FT−NMR spectra were measured with either a Bruker DRX400 or DMX500 instrument at 25 °C using chloroform-*d* ($CDCl_3$) as the solvent. Nondeuterated chloroform was used as an internal standard ($\delta = 7.26$ ppm).

Size Exclusion Chromatography. Size exclusion chromatography (SEC) was performed using a Knauer K-501 isocratic HPLC pump connected to a Knauer K-2301 differential refractometer. Separation was achieved using columns from Polymer Laboratories: two (2) PLGel 5 μm Mixed-D columns (linear range: 400−400 000 g/mol) and one (1) PLGel 5 μm 100 Å column connected in series. THF was used as the mobile phase at a flow rate of 1 mL/min at 25 °C. Molecular weight calibrations were made using Polymer Laboratory Easical PS-2 polystyrene calibration strips which cover a nominal molecular weight range of 580−400 000 g/mol.

Differential Scanning Calorimetry. DSC spectra were acquired on a dry nitrogen purged Perkin-Elmer DSC-7 equipped with an intercooler. The reported results are for the second scan from 0 to 200 °C at 10 °C/min after an initial thermal ramp from 25 to 200 °C at 50 °C/min, a 2 min isothermal hold at 200 °C, followed by a quench to 0 °C at 100 °C/min. No thermal transitions other than the glass transition were observed.

Sample Preparation. Thin films were made via spin-coating from 5% (w/w) toluene solutions at 2000 rpm for 45 s onto ~1 cm^2 silicon wafer substrates. All solutions were filtered using 0.22 μm Teflon syringe tip filters attached to a glass syringe prior to spin-coating. Sample substrates were cleaved from single side polished, (100) face, 3 in. diameter silicon wafers obtained from University Wafer. Prior to use, all substrates were cleaned by first dipping into hot acetone, then hot methanol and finally rinsing thoroughly with 18.2 MΩ cm deionized water obtained from a Millipore Milli-Q system. Sample films were vacuum annealed above their bulk glass transition temperature for 16 h at 65 °C and allowed to cool to room temperature under vacuum prior to surface analysis. Sample film thicknesses were determined from ellipsometry to be in the range of 180−220 nm using a Rudolph EL III fixed wavelength null ellipsometer equipped with a HeNe laser operating at 632.8 nm.

X-ray Photoelectron Spectroscopy. X-ray photoelectron spectroscopy (XPS) spectra were acquired on a Physical Electronics PHI ESCA 5500 system using a focused monochromated Al Kα (1486.6 eV) X-ray source operated at 15 kV at 350 W. High-resolution scans were done at a variety of tilt angles ranging from 8° to 72° and at a pass energy of 58.70 eV. A minimal amount of specimen neutralization was required in all cases and was accomplished utilizing a low-energy electron flood gun to maintain the aliphatic C 1s peak at ~285 eV. Multiple samples were used in order to minimize error from X-ray damage due to either fluorine loss or ester group degradation. Sample X-ray exposure time was kept to a maximum of 40 min for any sample. All spectra were analyzed and quantified using the manufacturer's software PHI-Multipak v.6.0a and their included atomic sensitivity factors. A further description of the XPS process is given in the Appendix.

Contact Angle. Water contact angle measurements were made using a Rame-Hart contact angle goniometer using 18.2 MΩ cm, 0.22 μm filtered deionized water obtained from a Millipore Milli-Q system as the probe liquid. Measurements were obtained at an ambient temperature of ~23 °C using 15 μL drops formed using a 25 μL Drummond positive displacement syringe. Drops were measured in an advancing mode and the reported results are the average of three separate drop measurements at different locations on the sample surface.

Results and Discussion

Polymer Synthesis and Characterization. Poly(D,L-lactide)s with low surface tension fluorocarbon groups located at either the chain end or chain center were synthesized via the ring-opening polymerization of lactide using tin(II) 2-ethyl hexanoate as the catalyst and either monofunctional or difunctional

Scheme 1. Synthesis of End and Center-Functional Poly(D,L-lactide)

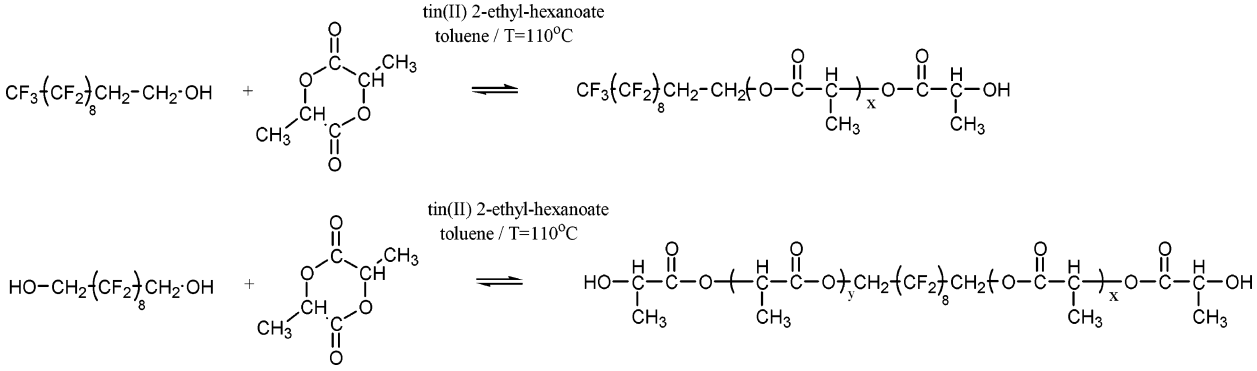

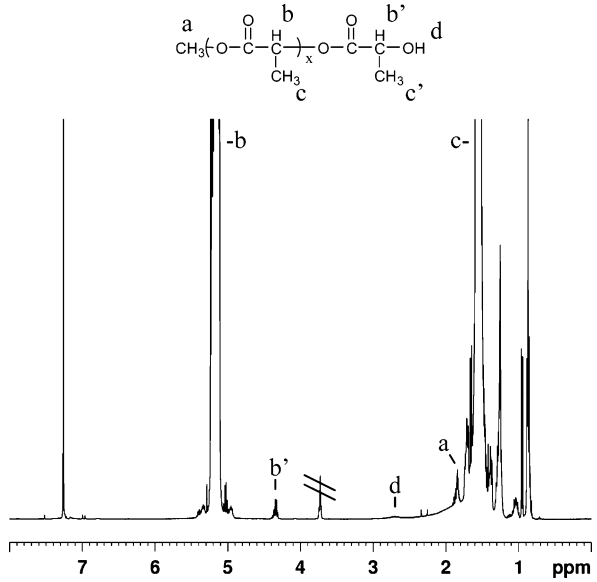

Figure 1. ^{1}H NMR spectrum in $CDCl_3$, of nonfunctional poly(D,L-lactide) (PLA19.5). Data: 1.35−1.90 [b, CH_3, lactic acid backbone], 2.70 [b, 1H, OH, terminal], 3.72 [m, THF solvent], 4.34 [m, 1H, CH, terminal lactic acid], and 4.90−5.50 ppm [b, CH, lactic acid backbone].

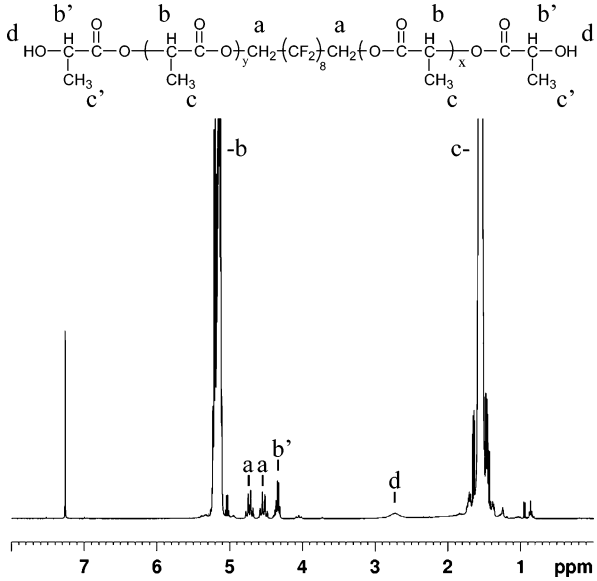

Figure 2. ^{1}H NMR spectrum CDCl3 of center-functional poly(D,L-lactide) (PLA5.9C). Data: 1.35−1.90 [b, CH3, lactic acid backbone], 2.70 [b, 1H, OH, terminal], 4.34 [m, 1H, CH, terminal lactic acid], 4.53 [m, 1H, CH2, initiator], 4.71 [m, 1H, CH2, initiator], and 4.90−5.50 ppm [b, CH, lactic acid backbone].

semifluorinated alcohols respectively as co-initiators (Scheme 1). The 50/50 racemic mixture of (D) and (L) enantiomers of the lactide was used as the monomer precursor in preference to either of the pure optical forms, as it has been shown that such mixtures yield an amorphous product.[21] Three molecular weights of both end-functional and center-functional poly(D,L-lactide)s (PDLLAs) were synthesized. The molecular weight was controlled by varying the monomer to initiator ratio at a fixed 1:5 catalyst to initiator ratio. A nonfunctional PDLLA to serve as a control was also synthesized using methanol as the initiator.

^{1}H NMR spectra of nonfunctional (PLA19.5), center-functional (PLA5.9C), and end-functional (PLA6.1E) PDLLAs are shown in Figures 1−3, respectively, with major peak assignments determined with the aid of the literature.[22−24] The number-average molecular weights were determined from the ratio of the signal intensities of protons in the initiator fragment

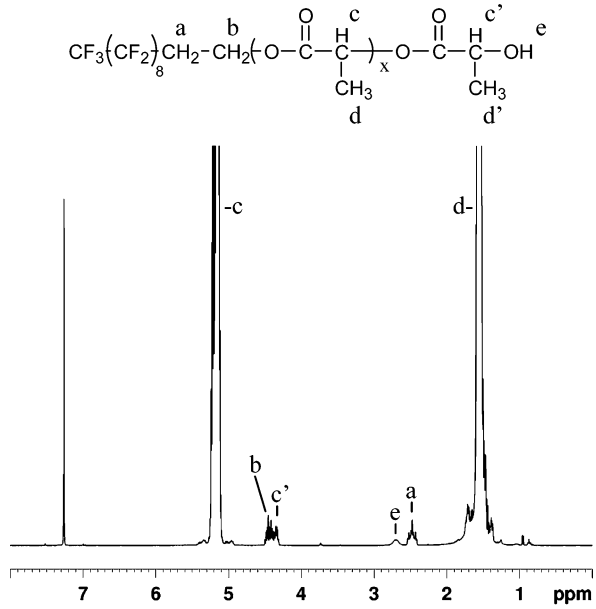

Figure 3. ^{1}H NMR spectrum in $CDCl_3$ of end-functional poly(D,L-lactide) (PLA6.1E). Data: 1.35−1.90 [b, CH_3, lactic acid backbone], 2.42−2.52 [m, 2H, CH_2, initiator], 2.70 [b, 1H, OH, terminal], 4.32−4.38 [m, 1H, CH, terminal lactic acid], 4.38−4.48 [m, 2H, CH_2, initiator], and 4.90−5.50 ppm [b, CH, lactic acid backbone].

Table 1. Characterization Results for Functional Poly(D,L-lactide)

polymer	M_n NMR	M_n SEC	functionality, f NMR	PDI SEC	T_g [°C] DSC	contact angle
PLA6.1E	6100	8400	0.96	1.24	35	91
PLA9.6E	9600	12 200	0.91	1.49	36	90
PLA16.5E	16 500	14 800	0.95	1.33	42	90
PLA5.9C	5900	6100	0.99	1.25	32	78
PLA10.0C	10 000	10 800	0.91	1.30	44	74
PLA15.4C	15 400	14 800	0.71	1.42	40	69
PLA19.5	19 500	24 000	N/A	1.63	41	68

to those from the methine group of the lactic acid repeats in the polymer backbone. The polymer functionalities were calculated from the ratios of the intensities of the initiator protons to the methine protons in the ω-terminal lactic acid repeat. Characterization results are shown in Table 1. The sample designation codes begin with PLA to denote poly(D,L-lactide), are then followed by the NMR number-average molecular weight in kilodaltons, and end with an E or C to indicate either an end-functional or center-functional polymer, respectively. The code PLA6.1E therefore refers to an end-functional poly(D,L-lactide) with a molecular weight of 6100.

ADXPS Surface Characterization. Figure 4 shows a high-resolution scan of the carbon 1s (C 1s) region for PLA6.1E obtained at takeoff angles of 16, 21, 32, and 72° as well as results obtained from the peak-fitting procedure for the 72° spectrum. Separate peaks can be resolved at binding energies of 284.8, 286.8, 288.9, 291.6, and 294.0 eV and have been assigned to the following chemical groups, respectively: −(CH)−(C*H_3)−(284.8), −(C*H)−O−(C═O)− (286.8), −(O═C*)−O−C− (288.9), −(C*F_2)− (291.6), and −(C*F_3) (294.0). The C 1s regions of the center-functional polymers are similar to the end-functional with the noted absence of the −(C*F_3) peak at 294.0 eV. The intensity of the −(C*F_2)− signal (the −(C*F_3) peak as well, in the case of the end-functional PDLLA) increases relative to the −(C*OO)− and −(C*O)− backbone polymer signals with decreasing takeoff angle, suggesting that the concentration of the semifluorinated functional groups is higher at the surface than in the bulk.

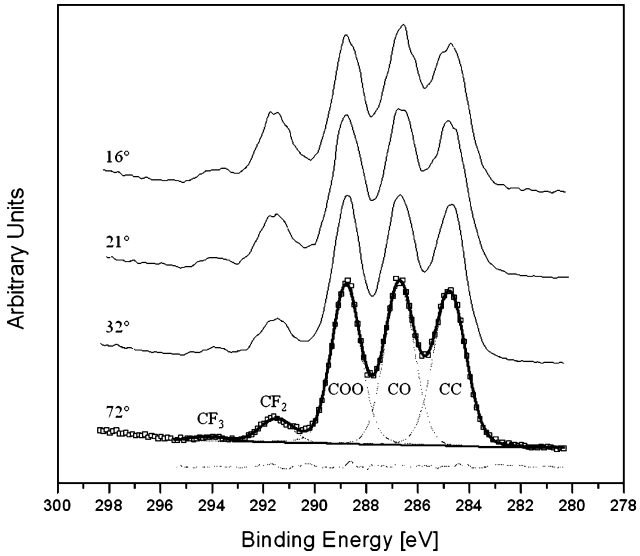

Figure 4. High-resolution XPS carbon 1s spectra for PLA6.1E at 16, 21, 32, and 72° photoelectron take off angles with peak-fitting results shown for the 72° spectrum.

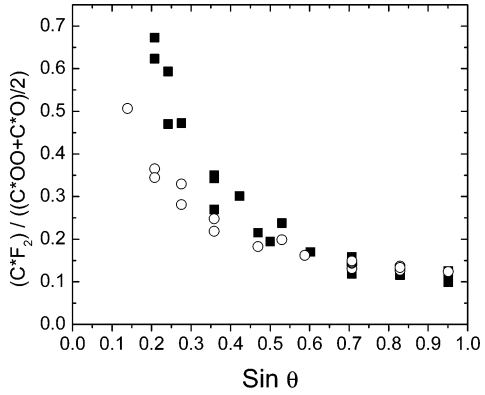

Figure 5. $(C^*F_2)/((C^*OO + C^*O)/2)$ ratio as a function of sin θ for PLA6.1E (filled squares) and PLA5.9C (open circles).

The influence of a variety of instrumental factors can be eliminated by using ratios of XPS signals emanating from different atomic species (see the Appendix). In the present case, it is convenient to use the ratio of an XPS signal associated with the functional group to one originating from the chain backbone. Figure 5 compares characteristic ADXPS concentration depth profile ratios [see (A17)] for PLA6.1E and PLA5.9C, functional polymers with similar overall volume fractions of functional groups. The $-(C^*F_2)-$ signal is used to reflect the concentration of fluorocarbon functional groups while the average of the $-(C^*OO)-$ and $-(C^*O)-$ signals is used as a measure of the concentration of lactic acid repeat units. These latter two chemical groups are present in a one to one molar ratio in the poly(D,L-lactide) chain backbone and are not found in the fluorinated functional group. The expected overall fraction of fluorocarbon groups is 0.09 for PLA6.1E and 0.105 for PLA5.9C.

The ADXPS results show that the lower surface tension fluorocarbon groups segregate preferentially to the surface for both polymer architectures. In each case, the integral concentration depth profiles show a maximum functional group concentration (i.e., fluorine concentration) at the surface with a monotonic decay in concentration as the depth is increased. The degree of surface segregation for the fluorocarbon groups is clearly greater for the end-functional polymer, consistent with the lattice model prediction that location of low surface tension functional groups at the chain ends provided for the highest degree of surface segregation.[16]

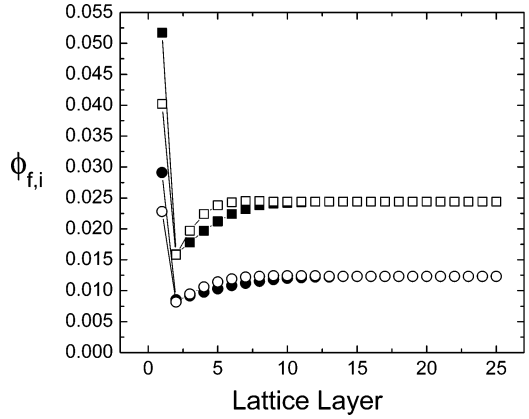

Figure 6. Functional group volume fraction profiles for two chain lengths of end-functional (closed symbols) and center-functional polymers (open symbols) with a single functional group for $\chi_s = -1$, $\chi_{bulk} = 1$, $f = 1$. The normalized chain lengths are $r = 41$ (squares), $r = 81$ (circles).

Water contact angles (see Table 1) for both the end-functional and center-functional polymers are higher than that of the nonfunctional PDLLA control consistent with segregation of the low surface tension fluorocarbon groups to the surface. The water contact angles for the center-functional polymers are also lower than those for the corresponding molecular weights of the end-functional polymers, indicating that a higher degree of surface segregation of fluorocarbon groups is achieved when they are placed at the chain end.

Lattice Model Calculations. The parameters required for the mean field lattice model (MFLM) calculation are as follows: the chain length of the functional polymer, the functionality of the functional polymer, the chain length of the nonfunctional polymer (if the functionality is less than unity), the surface interaction parameter, χ_s, and the bulk interaction parameter, χ_{bulk} (see the Appendix for model details). The MFLM calculations provide a prediction of the concentration depth profiles for the functional group and repeat units of each polymer. Because the functional and nonfunctional polymers have the same lactic acid repeat unit, the repeat unit volume fractions are added together to reduce the solution to concentration profiles for two constituents: the functional group and the repeat unit.

The general characteristics of "attractive" (i.e., $\chi_s < 0$) functional group distributions in end- and center-functional polymers predicted by the MFLM are shown in Figure 6. The volume fraction of functional groups in lattice layer i is denoted as $\phi_{f,i}$. The basic features of the functional group distributions are similar to those observed for neat end- and center-functional polymers.[16,20,25−28] Surface enrichment of the low surface tension functional groups is confined to the first lattice layer, while successively deeper layers exhibit a depletion gradient with gradually rising concentration over a depth comparable to the chain dimensions. The number of functional groups in the first lattice layer of the end-functional polymer is consistently higher than that for the center-functional polymer and as would be expected, an increase in the chain length results in a corresponding decrease in the bulk concentration of functional groups. If the lattice size is roughly equivalent to the statistical segment length, screening is expected for distances greater than one lattice layer such that the surface excess is observed only in the first lattice layer. The depths of the subsequent depletion layers scale with the chain dimensions, because chain con-

Table 2. Characteristic Monomer and Functional Group Parameters Calculated from Group Contribution Methods

Structure	Molar Volume [cm^3/mol]	Solubility Parameter [cal$^{1/2}$/cm$^{3/2}$]	Surface Tension γ [mN/m]	Surface Tension γ [mN/m]
End Group 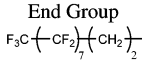	232.7 (VK[a])	6.9 (VK[a])	20.8 (H&S[a])	21.1 (K&S[a])
Center Group 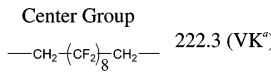	222.3 (VK[a])	6.7 (VK[a])	19.0 (H&S[a])	19.4 (K&S[a])
Lactic Acid 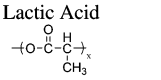	57.69[b]	9.9[c]	35.6[c]	

[a] Obtained from group contribution relations: VK = Van Krevelen,[30] H&S = Hildebrand and Scott,[31] and K&S = Koenhen and Smolder.[32] Included also are literature values of: [b]molar volume (calculated from the reciprocal of the measured density for amorphous poly(lactic acid) of 1.248 g/cm^3), [c]solubility parameter and surface tension.[33]

nectivity dictates that the overall composition must equal that of the bulk when integrated over a depth corresponding to the size of an individual polymer chain.

The nature of the depletion zone also differs between the two chain architectures, propagating further away from the surface for the end-functional polymer. Theodorou[26] showed that the presence of an interface causes bond orientations at the surface to depart from the isotropic distribution found in the unconstrained bulk. In the case of his AB_{r-1} system, analogous to our end-functional system, it was found that as χ_s increases, the increasing tendency of the surface active A end groups to adsorb to the surface caused chain congestion in subsequent layers. Elongated chain conformations perpendicular to the surface were enhanced with bonds directed perpendicular, rather than parallel, to the surface. In triblock copolymers of the type $B_{rB/2}A_{rA}B_{rB/2}$, similar to our center-functional case, Theodorou found the reverse to be true, near surface chains appeared flattened parallel to the surface. The flattening of chains near a surface has also been observed for the case of bulk homopolymer chains.[29] The increase observed in the depletion layer thickness is likely the result of a combination of these two factors: (a) the extension of the chains perpendicular to the surface in the near surface region in order to maximize the adsorption of functional chain-ends, (b) the tendency of chains to flatten parallel to the surface in the center-functional polymers.

Physically relevant ranges of χ_s and χ_{bulk} that are consistent with the known chemical structure of our polymers were determined prior to modeling. From the definitions of the interaction parameters, given in (A2) and (A3), values for both parameters may be calculated from either experimental measurements of the surface tension and solubility parameter obtained from the literature, or from values of these quantities calculated using group contribution methods.[30] A summary of some of the relevant modeling parameters, calculated for the end-functional and center-functional groups, along with literature data obtained for amorphous poly(lactic acid) is given in Table 2.

One of the limitations of rigid lattice theories is the necessity to define a single reference volume for a lattice site. In heterogeneous polymer systems the various constituents often have different volumes, rendering precise specification of the reference volume impossible. In the case of the functional PDLLAs, a partial resolution to this difficulty may be obtained by selecting the volume of the lactic acid repeat unit as the reference volume and then partitioning the fluorocarbon functional groups into segments of roughly equivalent volume, such that the average volume of each functional group segment is equivalent to that of the lactic acid repeat unit. This method has the drawback of possibly overestimating the entropy of the rigid fluorocarbon group, however proper estimation of the entropy of the much longer lactic acid backbone is more significant in determining the overall behavior of the chain. Recent work modeling the ADXPS data for *ω*-fluorosilane terminated poly(styrene) demonstrated that the partitioning method yielded reasonable results.[16]

Table 3. Relevant Physical Parameters of the End- and Center-Functional Poly(D,L-lactide)s Required for MFLM Calculations

polymer	M_n [g/mol] NMR	$n = (M_n - M_{init})/M_{repeat}$	r (funct polymer)	r (nonfunct polymer)	f NMR
PLA6.1E	6100	78	79	75	0.96
PLA9.6E	9600	128	126	122	0.91
PLA16.5E	16 500	223	218	214	0.95
PLA5.9C	6000	76	80	76	0.91
PLA10.0C	10 000	132	136	132	0.99
PLA15.4C	15 400	208	214	210	0.71

Subsequent modeling of the end- and center-functional PDLLAs used the volume of the lactic acid repeat unit (57.69 cm^3/mol) as the lattice reference volume. On the basis of the molar volumes calculated in the Appendix (Tables 4 and 5), fluorocarbon groups were divided into four segments in order to yield average functional group segment volumes (58.20 cm^3/mol for the fluorocarbon end group and 55.59 cm^3/mol for the center-functional group) that were a good match to the reference volume.

Modeling ADXPS Data for End- and Center-Functional PDLLA. The parameters required for the MFLM calculations are listed in Table 3. The number of lactic acid repeat units in each polymer, n, was calculated based on the number-average molecular weights obtained from ^{1}H NMR where: (a) M_{init} was the adjusted mass of the end and center initiator groups (minus one OH group), 447 and 445 g/mol, respectively and (b) the mass of a lactic acid repeat unit was 72 g/mol. The chain lengths for the end- and center-functional polymers, r, were then calculated according to (A1). Because the functionality of the polymers was not unity, the polymer was modeled as a mixture of functional and nonfunctional polymers, and thus the values of r for each polymer in the mixture are reported. All subsequent modeling assumes that the fluorocarbon functional groups occupy four lattice sites.

The basic characteristics of "attractive" functional group distributions in end- and center-functional polymers with four adjacent functional group segments shown in Figure 7 are similar to those reported previously for a single functional group. Surface enrichment of the four adjacent low-energy functional group segments is confined to the first lattice layer, while successively deeper layers exhibit a depletion gradient that gradually rises to the bulk concentration level. It is evident for both chain architectures, however, that the minimum in concentration observed is not as well-defined as it is for the case of the single functional group case, but is distributed more broadly over the second, third, and even fourth lattice layers. This behavior occurs because the functional group occupies four adjacent lattice sites in both architectures, and is similar to the behavior found for triblock copolymers.[26] Note that while the minimum in concentration now appears to be broader than for the case of a functional group occupying a single lattice site,

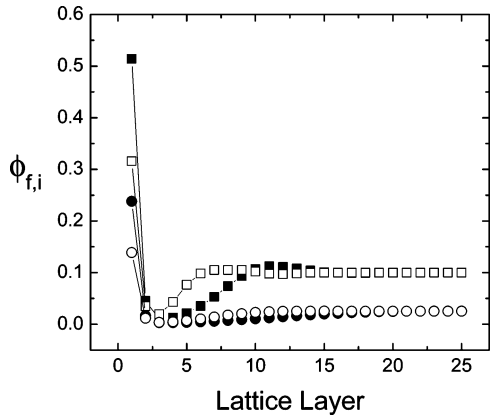

Figure 7. Functional group volume fraction profiles for two chain lengths of end- (closed symbols) and center-functional polymers (open symbols) when the functional group occupies four lattice sites for $\chi_s = -1$, $\chi_{bulk} = 1$, and $f = 1$. The normalized chain lengths are $r = 41$ (squares), $r = 161$ (circles).

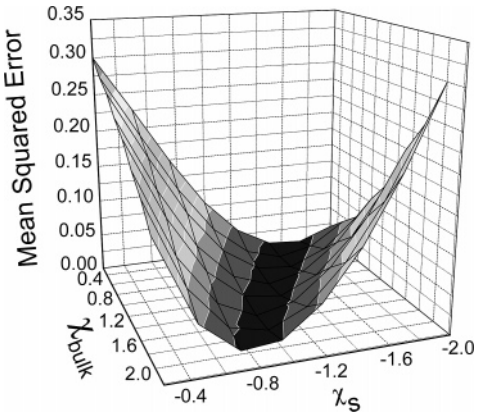

Figure 8. Sum of the mean-squared errors between MFLM predictions and observed ADXPS functional group depth profile ratios for end-functional poly(D,L-lactides): PLA6.1E, PLA9.6E and PLA16.5E.

the surface enrichment is still confined to the topmost lattice layer.

In order to obtain theoretical functional group composition profiles for the polymers studied, the surface and bulk interaction parameters were taken as adjustable parameters with their optimal values determined by simultaneous regression of the MFLM to the entire set of ADXPS data collected for all samples. Simulated MFLM functional group composition−depth profiles were subsequently used to calculate theoretical ADXPS atomic concentration ratios of $-(C^*F_2)-$ atoms present in the functional groups to (C*OO + C*O)/2 atoms present in the lactic acid backbone according to (A17). These ratios were calculated for sets of χ_s and χ_{bulk} values within the ranges $-0.25 < \chi_s < -2$ and $0 < \chi_{bulk} < 2$. The mean-squared errors between simulated and experimental ADXPS depth profile ratios were calculated and summed over all of the data sets at all photoelectron takeoff angles to obtain an overall mean squared error for each parameter set. The total mean-squared errors for the three molecular weights of end-functional PDLLAs are presented in Figure 8 as a function of χ_s and χ_{bulk}. The data do not show a global minimum, but rather a trough of roughly equivalent minimal mean-squared error. That is, many pairs of χ_s and χ_{bulk} values provide reasonable representations of the data. The general behavior of the center-functional PDLLAs is similar.

Only one set of parameters is thermodynamically consistent, however, because χ_s and χ_{bulk} are related. The relationship

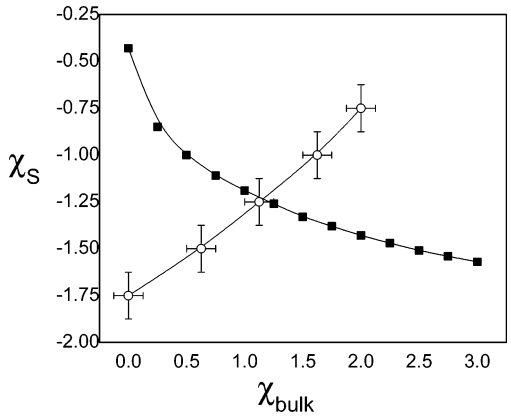

Figure 9. Relationship between χ_s and χ_{bulk}: (filled squares) predicted by the Hildebrand and Scott group contribution equations; (open circles) and obtained by regression of the ADXPS data for the end-functional poly(D,L-lactide)s to the MFLM.

between χ_s and χ_{bulk} can be established by group contribution methods. Group contribution methods provide relationships between the solubility parameter of the functional group and its surface tension.[30] Since χ_s and χ_{bulk} are functions of these same two variables, according to eqs A2 and A3, a group contribution relationship between χ_s and χ_{bulk} can be established. The theoretical relationship between χ_s and χ_{bulk} is obtained by application of the Hildebrand and Scott[31] group contribution equation for estimation of the surface tension of the functional group, γ_f, from the dispersive component of its solubility parameter, δ_{disp}, and its total molar volume, ν_f

$$\gamma_f = 0.07147(\delta_{disp})^2(\nu_f)^{1/3} \quad (1)$$

Since χ_s is related to γ_f by (A2) and γ_f to δ_{disp} by (1), one can derive a relationship between χ_s and δ_{disp}. Since χ_{bulk} is also related to δ_{disp} by (A3), one can then develop a direct group contribution relationship between χ_s and χ_{bulk}, which is plotted as the filled squares in Figure 9. The thermodynamically consistent pair of χ_s and χ_{bulk} values is then determined by the intersection of the experimental relationship between χ_s and χ_{bulk} obtained from the trough of minima in the ADXPS data regression (Figure 8) with the group contribution relationship between χ_s and χ_{bulk}. Figure 9 shows that the intersection provides a self-consistent set of optimal parameters: $\chi_s = -1.23$ and $\chi_{bulk} = 1.17$. Values for χ_s and χ_{bulk} can also be calculated directly from the chemical structures of the functional groups and repeat units using group contribution methods shown in the Appendix. The results of such calculations are summarized in Tables 4 and 5. The interaction parameters calculated from the group contribution equations are $\chi_s = -1.13$ and $\chi_{bulk} = 0.92$ for the end-functional polymers, in reasonable agreement with those furnished by the parametric optimization.

The final test of the MFLM is to examine whether it can reproduce all of the experimental ADXPS data. The ability of the two sets of interaction parameters to represent the experimental ADXPS data is shown in Figures 10 and 11, respectively, for the end-functional and center-functional PDLLAs. Both sets of interaction parameters provide acceptable representations of the experimental data for all molecular weights examined for both the end-functional and center-functional polymer chain architectures, with the profiles obtained from the group contribution method being overall slightly lower than those obtained from the global minimization of the ensemble of data. Further examination of the theoretical predictions suggest that there may

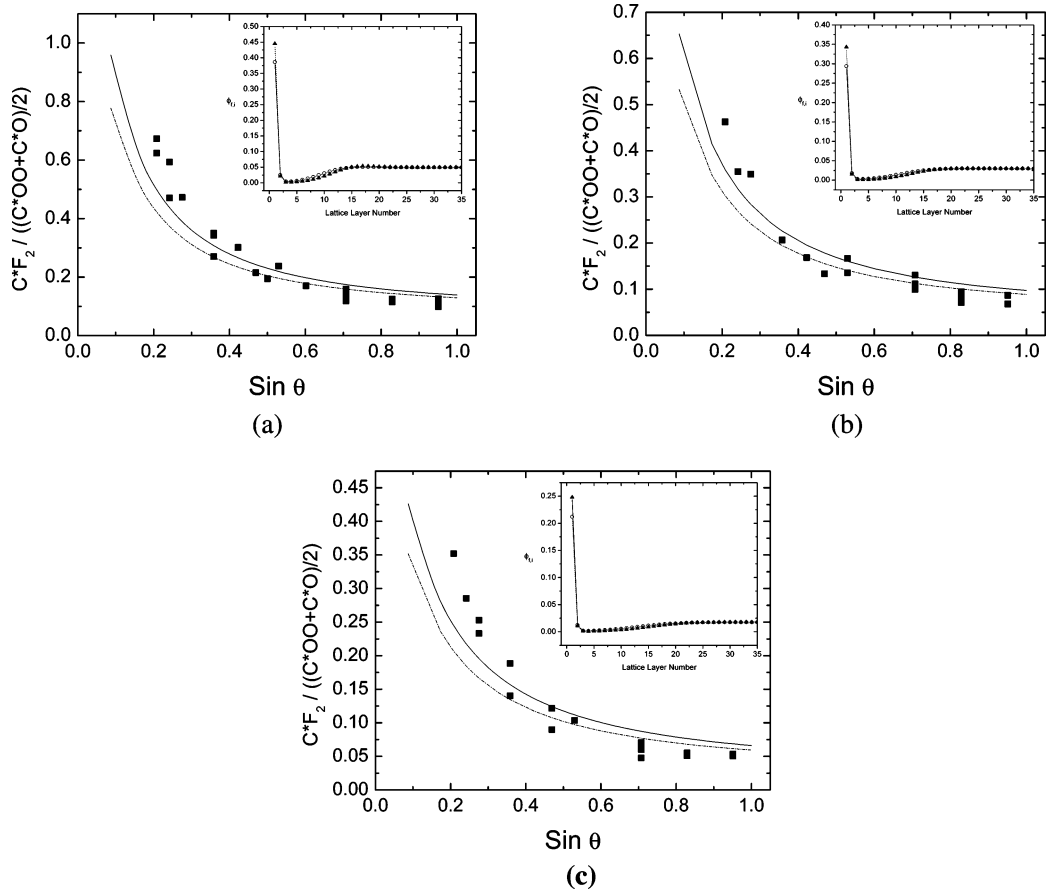

Figure 10. (C^*F_2) to ($C^*OO + C^*O$)/2 ratios as a function of the sine of the photoelectron takeoff angle for end-functional polymers. The solid lines are MFLM predictions using the values $\chi_s = -1.23$ and $\chi_{bulk} = 1.17$ obtained from the parametric fitting method while the dashed lines are the predictions using $\chi_s = -1.14$ and $\chi_{bulk} = 0.92$ calculated from the Hildebrand and Scott group contribution equations. The functional group is assumed to occupy four lattice sites. The insets show the predicted MFLM volume fraction profiles from the parametric method (solid up triangles) and the Hildebrand and Scott equations (open circles). (a) PLAEF6.1 treated as a blend of 96% end-functional polymer ($r = 79$) and 6% nonfunctional ($r = 75$) poly(D,L-lactide). (b) PLAEF9.6 treated as a blend of 91% end-functional polymer ($r = 126$) and 11% nonfunctional ($r = 122$) poly(D,L-lactide). (c) PLAEF16.5 treated as a blend of 95% end-functional polymer ($r = 218$) and 5% nonfunctional ($r = 214$) poly(D,L-lactide).

also be a general underestimation of the experimental data at low takeoff angles, however, given the magnitude of the errors inherent in obtaining XPS data at low takeoff angles due to variables such as surface roughness, photoelectron scattering and a relatively large detector solid angle, the level of agreement between the theory and experimental data is quite encouraging. On this basis we conclude that the surface properties of end-functional and center-functional polymers for a variety of molecular weights can thus be reasonably well predicted by the lattice model using parameters determined entirely from group contribution calculations.

The only proviso with use of the MFLM appears to be that the reference volume should be considered carefully when performing the calculations. If an appropriate volume for the polymer repeat unit is not used as the reference volume, the estimated number of lattice sites in the polymer chain will not be correct and the model calculations will be in error due to improper calculation of the chain entropy. In the present case, it is necessary to divide the functional group into four adjacent units in order to provide a good match between the volume of the repeat unit and the reference volume. This approach, however, may also lead to errors as it tends to underestimate the stiffness of the functional group. For the functional polymers studied herein, containing rather stiff fluorocarbon-based functional groups, there is a large mismatch between the stiffness (i.e., reference volumes) of the polymer chain and the functional group, making it difficult to assign an unambiguous reference volume. This asymmetry effect may provide some explanation for the tendency of the MFLM to underestimate the surface fraction of functional groups. That is, if the stiff fluorocarbon units tend to lie horizontally at the surface, the observed surface fluorocarbon content would be higher than expected from the flexible lattice model as appears to be observed. Unfortunately, asymmetry effects of this nature cannot be accounted for in an incompressible lattice theory with a single lattice volume. Additional experiments on other asymmetric systems would be necessary to determine the importance of asymmetry in these calculations.

Conclusions

Angle dependent X-ray photoelectron spectroscopy (ADXPS) has been employed to characterize functional group surface segregation and functional group surface composition−depth profiles for poly(D,L-lactide)s with fluorocarbon functional groups at both the chain end and center. The lower surface tension fluorocarbon groups preferentially segregate to the surface in all cases. The extent of surface segregation is found to decrease with molecular weight, consistent with a decrease in the bulk concentration of functional groups and is found to be greater for the end-functional than for the center-functional

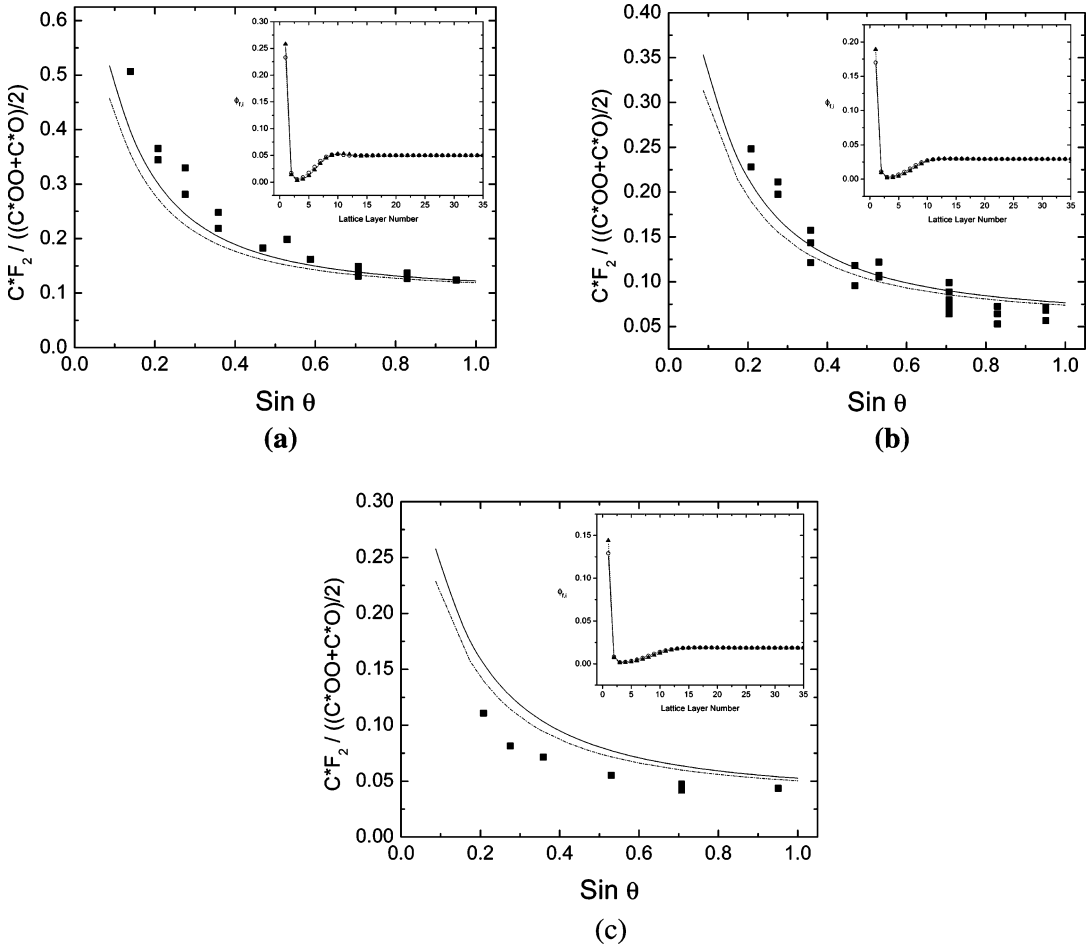

Figure 11. (C^*F_2) to ($C^*OO + C^*O$)/2 ratios as a function of the sine of the photoelectron takeoff angle for center-functional polymers. The solid lines are MFLM predictions using the values $\chi_s = -1.26$ and $\chi_{bulk} = 1.23$ obtained from the parametric fitting method while the dashed lines are the predictions using $\chi_s = -1.15$ and $\chi_{bulk} = 1.00$ calculated from the Hildebrand and Scott group contribution equations. The functional group is assumed to occupy four lattice sites. The insets show the predicted MFLM volume fraction profiles from the parametric method (solid up triangles) and the Hildebrand and Scott equations (open circles). Key: (a) PLACF6 treated as a blend of 91% center-functional polymer ($r = 80$) and 9% nonfunctional ($r = 76$) poly(D,L-lactide); (b) PLACF10 treated as a blend of 99% center-functional polymer ($r = 136$) and 1% nonfunctional ($r = 132$) poly(D,L-lactide); (c) PLACF16.5 treated as a blend of 71% center-functional polymer ($r = 214$) and 29% nonfunctional ($r = 210$) poly(D,L-lactide).

architecture for fixed molecular weight, consistent with the predictions of a mean field lattice model (MFLM). The experimental ADXPS integral concentration depth profiles for a variety of molecular weights of both end- and center-functional architectures can all be regressed to the MFLM using a single set of self-consistent surface and bulk interaction parameters provided that the reference volume is set equal to that of the lactic acid repeat unit. In this case, the fluorocarbon functional group is modeled as four adjacent units of average volume roughly equivalent to that of the repeat unit. The optimal surface and bulk interaction parameters obtained by this simultaneous regression procedure are in reasonable agreement with values estimated through group contribution methods.

Taken collectively, the results of this study demonstrate that (1) surface chemical composition and composition−depth profiles can be satifactorily predicted from the mean field lattice theory for a variety of functional polymer architectures and molecular weights and (2) that the surface and bulk interaction parameters necessary for these predictions can be adequately estimated by group contribution calculations based solely on the known chemical composition of the constituents.

Acknowledgment. This material is based upon work supported by, or in part by, U.S. Army Research Laboratory and the U.S. Army Research Office under Contract/Grant Nos. DAAD19-00-10104 in part by the National Science Foundation under Grant Nos. DMR-98-09687 and DMR-02-14263. Any opinions, findings, and conclusions or recommendations expressed in this material are those of the author(s) and do not necessarily reflect the views of the National Science Foundation.

Appendix

The information contained in this appendix on the mean field lattice model (MFLM), group contribution calculations and X-ray photoelectron (XPS) theory is provided as a convenience to the reader and contains work that has been published previously by our group.

Mean Field Lattice Model (MFLM). The framework for the calculations is the self-consistent mean-field lattice theory originally developed by Scheutjens and Fleer[20] to study adsorption in monodisperse polymer solutions in contact with an impenetrable, homogeneous surface. It is a mean-field lattice theory utilizing a number of assumptions: the lattice is assumed to be incompressible, the bulk phase is assumed to be

homogeneous, and the local concentration can be estimated from the bulk concentration. A similar approach was utilized by Hariharan et al. to study the surface properties of copolymers and binary polymer blends,[27,28,34−38] Theodorou to study the behavior of copolymers of arbitrary architecture near a hard surface,[25,26] and our own group to investigate the surface properties of α-functional and α,ω-functional polymers.[16,17,19,39,40] The basis of the model is a cubic lattice with layers parallel to and confined within two impenetrable walls that are sufficiently separated to provide a bulk like region in the center of the film. Properties are symmetric about the center of the film since the two walls are defined to be identical. The polymer system is modeled as incompressible which implies that each lattice site is occupied by a single chain segment. The functional polymer is placed on a cubic lattice such that the number of total chain segments, or normalized chain length, r, is then the total volume of the chain divided by the reference volume of a lattice site

$$r = \frac{n_r \upsilon_r + n_f \upsilon_f}{\upsilon_{ref}} \tag{A1}$$

where n_r is the number of backbone repeat units of volume υ_r, n_f is the number of functional groups of volume υ_f, and υ_{ref} is the reference volume for a lattice site. The lattice site volume is typically set equal to the volume of the polymer backbone repeat unit; however, sometimes it is more applicable to equate it to the volume of the functional group. If the functionality of the "neat" functional polymer is less than unity, it must be considered as a blend of functional polymer and nonfunctional polymer. In this case, the normalized chain length for the nonfunctional polymer is simply calculated from (A1) with $n_f = 0$. Surface segregation is governed by a balance between the resultant surface energy reduction and the required change in chemical potential associated with segregation of the functional group. The magnitude of the latter effect is related to the bulk interaction parameter, χ_b, between a functional group and the chain backbone.

The surface interaction parameter is related to the difference in adsorption energies of the functional group and a repeat unit segment

$$\chi_s = \frac{U_s^1 - U_s^2}{k_B T} = \frac{(\gamma_1 - \gamma_2)}{k_B T} \tag{A2}$$

where k_B is Boltzmann's constant, T is temperature in kelvin, and U_s^i is the change in energy associated with moving a segment of type i from the pure bulk to the surface. The latter adsorption energy is equal to the surface tension, γ_i, multiplied by the surface area per lattice site, which for a cubic lattice is $a = \upsilon_{ref}^{2/3}$. The surface interaction parameter is defined so that a positive value indicates that a functional group is repelled from the surface (repulsive or high surface energy functional group), while a negative value implies that functional groups are preferentially absorbed at the surface (attractive or low surface energy functional group).

Quantitative predictions of functional group concentration depth profiles must also consider the effects of bulk interactions between the functional group and the polymer backbone. The bulk interaction parameter can be calculated from regular solution theory, which should be applicable in the present case where only dispersive interactions are expected between the lactic acid backbone and the fluorocarbon functional group. The bulk interaction parameter can be estimated from solubility parameters according to

$$\chi_{bulk} = \upsilon_{ref}^{1/3} \frac{(\delta_f - \delta_r)^2}{N_A k_B T} \tag{A3}$$

where N_A is Avogadro's number, k_B is Boltzmann's constant, δ_f is the solubility parameter of the functional group, and δ_r is the solubility parameter of the repeat unit.

A zero-order continuation scheme is implemented to account for the bulk interactions when solving for the free segment probabilities in the lattice calculations. Calculations for a given chain length and χ_s value start with the bulk interaction parameter set to zero and then proceed to progressively increasing values of χ_s using the last solution as an initial guess for the next one. A step size of $\Delta\chi_s = 0.1$ proved to be adequate for this purpose.

Group Contribution Calculations. Surface and bulk interaction parameters for the functional groups as well as the repeat unit can be estimated by first applying group contribution methods to calculate the appropriate solubility parameters. The total solubility parameter, δ, as described by Hansen[41] can be described in terms of the different contributions due to dispersive (δ_{disp}), polar (δ_{polar}), and hydrogen-bonding (δ_{H-bond}) interactions:

$$\delta^2 = (\delta_{disp})^2 + (\delta_{polar})^2 + (\delta_{H-bond}) \tag{A4}$$

Following the method of Hansen, Hoftyzer, and Van Krevelen[42] proposed a methodology for estimating the three solubility parameters from group contributions based on molar attraction constants as first proposed by Small[43]

$$\delta_{disp} = \sum F_{i,disp}/\upsilon_m \tag{A5}$$

$$\delta_{polar} = \sum (F_{i,polar})^2/\upsilon_m \tag{A6}$$

$$\delta_{H-bond} = \sum F_{i,H-bond}/\upsilon_m \tag{A7}$$

where υ_m is the molar volume of the segment under consideration. Each segment is considered to comprise a number of subunit fragments, i, with molar attraction constants $F_{i,disp}$, $F_{i,polar}$, and $F_{i,H-bond}$ for dispersion, dipole, and hydrogen bond forces, respectively, and the solubility parameters are calculated by summing over the contributions of each subunit. For our purposes the polar and H-bonding components can be neglected for the semifluorinated functional groups as the interactions should be only of a dispersive nature. Once the solubility parameters of the functional group are calculated, the surface tension can be estimated by applying further group contribution relationships such as those proposed by Hildebrand and Scott[31]

$$\gamma_f = 0.07147(\delta_{disp})^2(\upsilon_f)^{1/3} \tag{A8}$$

or Koenhen and Smolder[32]

$$\gamma_f = (\delta_{disp}{}^2 + \delta_{polar}{}^2)(\upsilon_f)^{1/3}/13.8 \tag{A9}$$

where υ_f, is the molar volume of the functional group in question.

In this work the functional groups are assumed to occupy four adjacent lattice sites of approximately equivalent molar volume similar to that of the lactic acid repeat unit. The functional groups were divided so as to incorporate full chemical

Table 4. Molar Volume, Solubility Parameter, Surface Tension, χ_s, and χ_{bulk} Calculated from Group Contribution Methods for the Four-Adjacent End-Functional Semifluorinated Groups[a]

structure functional group	CF_3-CF_2	CF_2-CF_2-CF_2	CF_2-CF_2	CF_2-CH_2·CH_2	av
molar vol [cm^3/mol] (VK)	57.68	71.10	47.40	56.44	58.20
solubility parameter [$cal^{1/2}/cm^{3/2}$](VK)	7.36	6.39	6.39	7.40	
surface tension γ [mN/m] (H&S)	14.96	12.1	10.57	14.99	
surface tension γ [mN/m] (K&S)	15.17	12.27	10.72	15.20	
χ_{bulk}	0.63	1.48	0.99	0.60	0.92
χ_s (H&S)	−1.05	−1.37	−1.12	−1.03	−1.14
χ_s (K&S)	−1.04	−1.36	−1.11	−1.02	−1.13

[a] VK = Van Krevelen,[30] H&S = Hildebrand and Scott,[31] K&S = Koenhen and Smolder.[32]

Table 5. Molar Volume, Solubility Parameter, Surface Tension, χ_s, and χ_{bulk} Calculated from Group Contribution Methods for the Four-Adjacent Center-Functional Semifluorinated Groups[a]

structure functional group	CH_2-CF_2	$CF_2-CF_2-CF_2$	$CF_2-CF_2-CF_2$	CH_2-CF_2	av
molar vol [cm^3/mol] (VK)	40.07	71.10	71.10	40.07	55.59
solubility parameter [$cal^{1/2}/cm^{3/2}$](VK)	7.10	6.39	6.39	7.10	
surface tension γ [mN/m] (H&S)	12.33	12.10	12.10	12.33	
surface tension γ [mN/m] (K&S)	12.50	12.27	12.27	12.50	
χ_{bulk}	0.53	1.48	1.48	0.53	1.00
χ_s (H&S)	−0.93	−1.37	−1.37	−0.93	−1.15
χ_s (K&S)	−0.92	−1.36	−1.36	−0.92	−1.14

[a] VK = Van Krevelen,[30] H&S = Hildebrand and Scott,[31] K&S = Koenhen and Smolder.[32]

moieties, such as $-(CH_2)-$ and $-(CF_2)-$, which have tabulated group contribution values, and as such the volumes of each group are not identical. In the group contribution calculations, the relevant solubility parameters and surface tensions were calculated according to the structure and associated molar volumes of the individual groups as defined in Tables 4and 5. These values in turn were used to calculate the interaction parameters χ_s and χ_b, according to (A2) and (A3) respectively, for each of the four units of the functional groups. Finally, the four individual interaction parameter values were then averaged to yield the final interaction parameters used in the lattice model calculations. Note that since the values of χ_s obtained from both the Hildebrand and Scott and Koenhen and Smolder group contribution methods are essentially equivalent, only the former values are used in the preceding calculations and discussions. Parameters employed for the lactic acid repeat unit were obtained from the literature: molar volume = 57.69 cm^3/mol (calculated from the reciprocal of the measured density for amorphous poly(lactic acid), 1.248 g/cm^3), solubility parameter = 9.9 $cal^{1/2}/cm^{3/2}$ and surface tension γ = 35.6 mN/m.[33]

X-ray Photoelectron Spectroscopy (XPS). In the XPS process an incident X-ray photon ejects a photoelectron from an atom's core atomic levels. If the incident X-ray photon energy is greater than the electron's binding energy, then this photoelectron is ejected with a certain kinetic energy, which is described by

$$E_{i,k} = h\upsilon - \mathrm{BE} - \mathrm{WF} \tag{A10}$$

where h is Planck's constant, BE is the binding energy of the electron (specific to the atom and orbital), $h\nu$ is the energy of the incident X-rays, and WF is the spectrometer's work function. The binding energy is specific to the type of atom and the orbital from which the electron originated and as such for a given X-ray photon energy, the kinetic energy of the ejected photoelectron $E_{i,k}$ is also specific to the atom i and orbital k from which the photoelectron originated.

The soft X-rays used in XPS penetrate many microns into a material but the information obtained from XPS is usually confined to a region less than 20 nm from the sample surface. This surface sensitivity arises from the much higher probability of interaction of electrons with matter than X-rays. The probability of photoelectron escape without inelastic collision is $e^{-z/\lambda\sin\theta}$ where z is the depth, λ is the electron mean free path, and θ is the photoelectron takeoff angle between the detector and the plane of the surface. An escape depth from which 95% of the photoelectrons emanate can therefore be defined as $d = 3\lambda \sin\theta$. Depth profiling is accomplished by varying the takeoff angle, with lower takeoff angles corresponding to shallower depths. The resultant ADXPS integral depth profile is of the form[40,44]

$$N_{i,k}(\theta) = I_0 K_{i,k} \lambda_{i,k} \int_0^\infty n_i(z) \exp(-z/\lambda_{i,k}\sin\theta)\, dz \tag{A11}$$

where $N_{i,k}^{\infty}$ is the measured photoelectron peak intensity from a k shell of an i type of atom, I_0 is the incident X-ray flux, $K_{i,k}$ is a sensitivity factor which in this case includes both the photoelectron ionization cross section and angular asymmetry parameter as well as instrumental factors such as the transmission function, $n_i(z)$ is the volume density of atom type i [atoms/cm^3] as a function of depth z, $\lambda_{i,k}$ is the inelastic mean-free path (IMFP) of the i,k photoelectrons in the sample. There are several expressions available in the literature for calculating photoelectron mean free paths. For example, IMFPs in this work were calculated based on the following relation proposed by Ashley and co-workers for polymers[45]

$$\lambda = (M/\rho n)E_k/(13.6\ln(E_k - 17.6 - 1400/E_k)) \tag{A12}$$

where M is the molar mass of the repeat unit, n is the number of valence electrons in the repeat unit, ρ is the mass density and E_k is the kinetic energy of the photoelectron in eV.

Simulating ADXPS Concentration Depth Profiles. To evaluate the integral in (A11), the polymer surface region is divided into a number of discrete layers of equal thickness, t, as in the lattice model. The layers are counted from the surface ($L = 1$) to some arbitrary layer within the bulk ($L = n$). Because the composition−depth profiles provided by the lattice model are discretized with a depth increment given by the lattice dimension, it is convenient to set the layer thickness equal to the lattice dimension in the lattice model, that is, $t = \upsilon_{ref}^{1/3}$. To compare the results of the lattice theory to experimental ADXPS data, the concentration n of element i within a given layer L,

$n_i(L)$, is first calculated using the outputs of the lattice theory. Starting with the first layer, (A11) is applied, integrating from the surface ($z = 0$) to the bottom of the first layer ($z = t$), to yield an expression for the signal intensity, $N_{i,k}(1)$, emanating from the first layer:

$$N_{i,k}(1) = K_{i,k}\lambda_{i,k}n_i(1)(\sin\theta)\left[1 - \exp\left(\frac{-t}{\lambda_{i,k}\sin\theta}\right)\right] \quad \text{(A13)}$$

For the second layer, the attenuation due to inelastic scattering in the overlayer must be taken into account, yielding

$$N_{i,k}(2) = K_{i,k}\lambda_{i,k}n_i(2)(\sin\theta)\left[1 - \exp\left(\frac{-t}{\lambda_{i,k}\sin\theta}\right)\right] \exp\left(\frac{-t}{\lambda_{i,k}\sin\theta}\right) \quad \text{(A14)}$$

A general expression for the signal intensity emanating from any layer, L, can therefore be written as

$$N_{i,k}(L) = K_{i,k}\lambda_{i,k}n_i(L)(\sin\theta)\left[1 - \exp\left(\frac{-t}{\lambda_{i,k}\sin\theta}\right)\right] \exp\left(\frac{t(1-L)}{\lambda_{i,k}\sin\theta}\right) \quad \text{(A15)}$$

By taking the sum of the intensities of all layers, the total signal intensity from element i at a particular takeoff angle, θ, is obtained:

$$N_{i,k}(L) = K_{i,k}\lambda_{i,k}\sum_{L=1}^{L=n} n_i(L)(\sin\theta) \left[1 - \exp\left(\frac{-t}{\lambda_{i,k}\sin\theta}\right)\right]\exp\left(\frac{t(1-L)}{\lambda_{i,k}\sin\theta}\right) \quad \text{(A16)}$$

In presenting and analyzing ADXPS data, it is common to report the ratio of signals for two elements because this representation eliminates a number of uncertainties such as variations in incident X-ray flux. In the case of functional polymers, the ratio of a signal associated with an atom in the functional group, *a*, to one associated with an atom in the chain backbone, *b*, is typically reported. Extension of the treatment presented above yields the following expression for the ratio of signals from two such atoms *a* and *b*:

$$\frac{N_a(\theta)K_b\lambda_b = \sum_{L=1}^{L=n} n_a(L)(\sin\theta) \left[1 - \exp\left(\frac{-t}{\lambda_a\sin\theta}\right)\right]\exp\left(\frac{t(1-L)}{\lambda_a\sin\theta}\right)}{N_b(\theta)K_a\lambda_a = \sum_{L=1}^{L=n} n_b(L)(\sin\theta) \left[1 - \exp\left(\frac{-t}{\lambda_b\sin\theta}\right)\right]\exp\left(\frac{t(1-L)}{\lambda_b\sin\theta}\right)} \quad \text{(A17)}$$

The inputs that are required to calculate the signal intensity ratio for these two signals include the composition in each lattice layer $n_i(L)$ (supplied by the lattice theory calculations), the takeoff angle used in the experiment θ, the IMFP for each signal λ_i (obtained from a relation such as (A12)) and the lattice layer thickness t which is set equal to the cube root of the reference volume used to define one cubic lattice site from the lattice theory.

References and Notes

(1) Bhatia, Q. S.; Pan, D. H.; Koberstein, J. T. *Macromolecules* **1988**, *21*, 2166−2175.
(2) Pan, D. H. K.; Prest, W. M., Jr. *J. Appl. Phys.* **1985**, *58*, 2861−2870.
(3) Jannasch, P. *Macromolecules* **1998**, *31*, 1341−1347.
(4) Jerome, R.; Teyssie, P.; Pireaux, J. J.; Verbist, J. J. *Appl. Surf. Sci.* **1986**, *27*, 93−105.
(5) Jones, R. A. L.; Kramer, E. J.; Rafailovich, M. H.; Sokolov, J.; Schwarz, S. A. *Phys. Rev. Lett.* **1989**, *62*, 280−283.
(6) Koberstein, J. T.; Duch, D. E.; Hu, W.; Lenk, T. J.; Bhatia, R.; Brown, H. R.; Lingelser, J. P.; Gallot, Y. *J. Adhes.* **1998**, *66*, 229−249.
(7) Jalbert, C.; Koberstein, J. T.; Hariharan, A.; Kumar, S. K. *Macromolecules* **1997**, *30*, 4481−4490.
(8) Jalbert, C. J.; Koberstein, J. T.; Balaji, R.; Bhatia, Q.; Salvati, L., Jr.; Yilgor, I. *Macromolecules* **1994**, *27*, 2409−2413.
(9) Elman, J. F.; Johs, B. D.; Long, T. E.; Koberstein, J. T. *Macromolecules* **1994**, *27*, 5341−5349.
(10) Forrey, C.; Koberstein, J. T.; Pan, D. H. *Interface Sci.* **2003**, *11*, 211−223.
(11) Affrossman, S.; Hartshorne, M.; Kiff, T.; Pethrick, R. A.; Richards, R. W. *Macromolecules* **1994**, *27*, 1588−1591.
(12) Schaub, T. F.; Kellogg, G. J.; Mayes, A. M.; Kulasekere, R.; Ankner, J. F.; Kaiser, H. *Macromolecules* **1996**, *29*, 3982−3990.
(13) Hopkinson, I.; Kiff, F. T.; Richards, R. W.; Budknall, D. G.; Clough, A. S. *Polymer* **1997**, *38*, 87−98.
(14) Hopken, J.; Moller, M. *Macromolecules* **1992**, *25*, 1461−1467.
(15) Gaines, G. L., Jr. *J. Phys. Chem.* **1969**, *73*, 3143−3150.
(16) O'Rourke-Muisener, P. A. V.; Koberstein, J. T.; Kumar, S. *Macromolecules* **2003**, *36*, 771−781.
(17) Muisener, P. A. V. O. R.; Jalbert, C. A.; Yuan, C.; Baetzold, J.; Mason, R.; Wong, D.; Kim, Y. J.; Koberstein, J. T.; Gunesin, B. *Macromolecules* **2003**, *36*, 2956−2966.
(18) Mason, R.; Jalbert, C. A.; O'Rourke, Muisener, P. A. V.; Koberstein, J. T.; Elman, J. F.; Long, T. E.; Gunesin, B. Z. *Adv. Colloid Interface Sci.* **2001**, *94*, 1−19.
(19) Jalbert, C.; Koberstein, J. T.; Yilgor, I.; Gallagher, P.; Krukonis, V. *Macromolecules* **1993**, *26*, 3069−3074.
(20) Scheutjens, J. M. H. M.; Fleer, G. J. *J. Phys. Chem.* **1979**, *83*, 1619−1635.
(21) Engelberg, I. a. K. *J. Biomaterials* **1991**, *12*, 292.
(22) Lee, W.-K.; Toselli, M.; Gardella, J. A., Jr. *Macromolecules* **2001**, *34*, 3493−3496.
(23) Stridsberg, K.; Ryner, M.; Albertsson, A.-C. *Macromolecules* **2000**, *33*, 2862−2869.
(24) Korhonen, H.; H. A.; Seppala, J. V. *Polymer* **2001**, *42*, 7541−7549.
(25) Theodorou, D. N. *Macromolecules* **1988**, *21*, 1411−1421.
(26) Theodorou, D. N. *Macromolecules* **1988**, *21*, 1422−1436.
(27) Hariharan, A.; Kumar, S. K.; Russell, T. P. *Macromolecules* **1991**, *24*, 4909−4917.
(28) Hariharan, A.; Kumar, S. K.; Russell, T. P. *Macromolecules* **1990**, *23*, 3584−3592.
(29) Theodorou, D. N. *Macromolecules* **1988**, *21*, 1400−1410.
(30) Van Krevelen, D. W. *Properties of Polymers: Their Correlation With Chemical Structure; Their Numerical Estimation and Prediction from Additive Group Contributions*, 3rd ed.; Elsevier: New York, 1997.
(31) Hildebrand, J. H. S.; R.L. *The Solubility of Non-electrolytes*; D. Van Nostrand: Princeton, NJ, 1950.
(32) Koenhen, D. M.; Smolders, C. A. *J. Appl. Polym. Sci.* **1975**, *19*, 1163−1179.
(33) Mark, J. E. *Polymer Data Handbook*; Oxford University Press: New York, 1999.
(34) Hariharan, A.; Harris, J. G. *J. Chem. Phys.* **1994**, *101*, 3353−3366.
(35) Hariharan, A.; Harris, J. G. *J. Phys. Chem.* **1995**, *99*, 2788−2796.
(36) Hariharan, A.; Kumar, S. K.; Rafailovich, M. H.; Sokolov, J.; Zheng, X.; Duong, D.; Schwarz, S. A.; Russell, T. P. *J. Chem. Phys.* **1993**, *99*, 656−663.
(37) Hariharan, A.; Kumar, S. K.; Russell, T. P. *J. Chem. Phys.* **1993**, *99*, 4041−4050.
(38) Hariharan, A.; Kumar, S. K.; Russell, T. P. *J. Chem. Phys.* **1993**, *98*, 6516−6525.
(39) Jalbert, C. A. In Ph.D. Dissertation; University of Connecticut: Storrs, CT, 1993.
(40) Fadley, C. S. *Prog. Surf. Sci.* **1984**, *16*, 275−388.
(41) Hansen, C. M. *J. Paint Technol.* **1967**, *39*, 104.
(42) Hoftyzer, P. J.; Van Krevelen, D. W. In *Properties of Polymers, Their Estimation and Correlation with Chemical Structure*, 2nd ed.; Elsevier: New York, 1976.
(43) Small, P. A. *J. Appl. Chem.* **1953**, *3*, 71.
(44) Andrade, J. D. *Surface and interfacial aspects of biomedical polymers*; Plenum Press: New York, 1985.
(45) Ashley, J. C. *IEEE Trans. Nucl. Sci.* **1980**, *NS-27*, 1454−1458.

MA0606915